Effect of nanoparticle clustering on the effective thermal conductivity of concentrated silica colloids

Chunwei Wu,[1] Tae Joon Cho,[2] Jiajun Xu,[1] Donggeun Lee,[3] Bao Yang,[1] and Michael R. Zachariah[1,2,*]

[1]*Department of Mechanical Engineering, University of Maryland, College Park, Maryland 20742, USA*
[2]*National Institute of Standards and Technology, Gaithersburg, Maryland 20899, USA*
[3]*School of Mechanical Engineering, Pusan Clean Coal Center, Pusan National University, Busan 609-735, South Korea*

Recent research on nanofluids has offered particle clustering as a possible mechanism for the abnormal enhancement of the effective thermal conductivity (k) when nanoparticles are dispersed in liquids. This paper was devoted to verify experimentally and theoretically the significance of the effect by altering the cluster structure, size distribution, and thermal conductivity of solid particles in water. Starting with well dispersed SiO_2 sols in water as a reference system, we control the aggregation kinetics by adjusting pH. Contrary to previous model predictions, the present experiment showed that clustering did not show any discernable enhancement in the thermal conductivity even at high volume loading. A series of fractal model calculations not only suggested that the conductive benefit due to clustering might be completely compensated by the reduced convective contribution due to particle growth, but also recommended the need for higher thermal conductivity and optimized fractal dimension of particles for maximizing the clustering effect.

PACS number(s): 82.70.−y, 65.80.−g, 82.60.Qr

I. INTRODUCTION

Nanofluids, i.e., solid-liquid composite suspensions, have attracted considerable research interest due to the anomalously increased thermal properties over the base fluids. This enhanced thermal conductivity makes them potentially attractive as heat transfer fluids for thermal management applications, e.g., cooling of microelectronics, transportation, solid-state lighting, etc.

Despite many investigations aimed at elucidating the unusual phenomenon behind nanofluids, a general agreement on the mechanisms responsible for the enhanced thermal transport has not yet emerged. Early experimental analyses and theoretical calculations of the thermal conductivity in solid/liquid heat-transfer fluids are largely dependent on the effective medium theory, which is basically categorized into the Maxwell-Garnett (M-G) model [1] and the Bruggeman model [2], which were originally developed for the study of the dielectric properties of composite consisting of host and inclusion phase. For instance, the Hamilton-Crosser (H-C) [3], deduced from the Maxwell rule by assuming that heat transport in each component is described by a diffusion equation, is very successful in predicting the thermal conductivity enhancement as a function of particle volume loading in large-sized particle suspensions. However, when dealing with nanofluids, the H-C model, with only macroscopic and diffusive heat transport under consideration, becomes inapt because it does not take into account particle size effect and further, it is adequate only for diluted suspensions. Compared to the M-G model, the Bruggeman model offers distinct advantages, e.g., applicable to nanofluids with a wide range of inclusion concentrations and capable of taking into account heat percolation through clustered aggregate structure [4,5].

The role of thermal Brownian motion of nanoparticles in nanofluids is still controversial. Additional heat advection by moving particles was anticipated to occur so that effective thermal conductivity of nanofluids is increased; however, this expectation was negated by Keblinski *et al.* who compared the characteristic time for Brownian diffusion of particles and heat conduction by the liquid and concluded that heat transport due to Brownian motion was negligible [6]. More recently, Jang and Choi proposed that heat could be additionally transferred by a localized microconvection associated with the fluid surrounding each random-moving particle [7]. By visualizing dye molecules, Prasher *et al.* experimentally confirmed that the mass transport was enhanced in nanofluids and suggested that particle motion might promote the convective thermal transport from analogy between convective heat and mass transfer [8]. In addition, their theoretical study strengthens the argument for the microconvective mechanism [9]. A recent experiment showed that the thermal conductivity decreased gradually and then approached the Maxwell limit with increasing the viscosity of the base fluid, in which the viscosity is solely tuned by volumetric fractions of the two constituent fluids that possess quite close thermal conductivity but very different viscosity [10]. This would be a significant indirect evidence of the Brownian motion effect.

The effect of particle clustering and its associated percolation has also been correlated with the enhancement of thermal transport, because when particles cluster into percolating networks, more efficient paths of lower thermal resistance could be created. Although a volume fraction of ∼15% is required for the percolation threshold for random dispersions, some local clustering is possible at lower volume loading [6] and was suggested to be another possible mechanism [4,6,11]. While classical theory to deal with percolation effect has been relatively well developed since 1987 [12,13], experimental works to prove it are still in their infancy. To our knowledge, Prasher's experiment is the only one dealing with particle clustering effects on thermal conductivity [4].

*mrz@umd.edu

However, their experiment was not made at high volume loading where the effects are expected to be stronger.

In this work, we have conducted a systematic study to clarify the effect of aggregation on the effective thermal conductivity of silica nanofluids particularly at high volume loading. We have chosen a SiO_2 colloid as a model system for the following reasons. First, the colloid containing size-monodisperse nonaggregated spherical particles was highly stable even at very high concentration (40 wt %) corresponding to a volume fraction ϕ of 23.3%. Such a good suspension of monomer particles has been hardly achieved by the previous researchers who have mixed commercial nanopowder with a liquid under strong ultrasonic agitation. These colloids often showed a severe aggregation and sedimentation of particles without control even at a few percent of volume fraction, which raised issues of aggregation state evolving during thermal conductivity measurements [14] and of artifacts associated with flocs' deposition on the surface of the measuring device and sedimentation of large clusters [4]. Second, the size distribution of particles in liquid could be well controlled from monomer particles of ca. 15 nm to large aggregates of several hundreds of nanometers. This wide spectrum in size is crucial for the study of the clustering effect. Using this well-defined system, we explored the size-related clustering effect of silica-water nanofluids and then evaluated the most recent general model proposed by Prasher *et al.* [4]. Next, using the model, we investigated the effectiveness of the clustering effect in terms of thermal conductivity and microstructure of particles.

II. EXPERIMENTAL

A commercial concentrated silica colloid (ST-40, Nissan Chemical America) with a mean diameter of 15 nm at 40 wt % was used as a model nanofluid system in this study. As-received concentrated dispersion shows no visible flocs or sediments, and the mass/volume fraction was further calibrated and verified by weighing a known volume of sample fluid before and after drying it.

The pristine colloid from the supplier was kept highly stable at relatively high *p*H (=10.1) where the negative charges serving as repulsive barrier were built on silica surface due to the ionization of residual silanol groups ($-SiOH$) through a dynamic balance of $-SiOH+OH^- \rightleftharpoons -SiO^-+H_2O$. When adding acid, neutralization of OH^- decreased the surface charge and zeta potential and thereby reduced the interparticle repulsive barrier. Further lowering the *p*H over the isoelectric point (IEP) leads to a gradual increase in the surface charge over zero to positive through another balance of $-SiOH+H_3O^+ \rightleftharpoons -SiOH_2^+ +H_2O$. In this regard, *p*H was chosen in our experiment to control the degree of aggregation by dropwise addition of concentrated HCl aqueous solution ($\sim$10 wt %) under vigorous stirring. It is noted that the tiny amount of HCl addition does not cause any undesired change in volume fraction.

The hydrodynamic diameters of the silica particles in liquid were determined by dynamic light scattering (DLS) with a Zetasizer Nano series (Malvern Instrument) with 633 nm laser (backscattering at 173° angle). All measurements were conducted at 20 °C after 2000 times dilution with buffer solutions at equal *p*Hs, which enables us to freeze-in the aggregation state at each condition. The DLS can give a great benefit of direct size measurement of particles in liquid as it is, with high sensitivity to cluster mass/volume distribution.

The effective viscosity of the silica colloids at various *p*Hs was directly measured by a digital viscometer (Brookfield DV-I PRIME) that has accuracy of 1.0% and repeatability of 0.2% in full scale range. The thermal conductivity of the colloids was measured at 20 °C using a 3ω-wire technique [15], a combination of the well-developed hot wire method and the 3ω method. In the 3ω-wire method, a metal wire is immersed into the liquid sample acting as both a heater and a thermometer. The method detects the frequency dependence, rather than the time dependence, of temperature oscillation in the metal wire through which a sinusoidal current at frequency ω is passed followed by generation of a 2ω-frequency heat wave in the fluid. The effective thermal conductivity k of the fluid is determined from the slope of the 2ω-temperature rise,

$$k = \frac{p}{4\pi l}\left(\frac{\partial T_{2\omega}}{\partial In\omega}\right)^{-1},$$

where p is the applied electric power, ω is the frequency of the applied electric current, l is the length of the metal wire, and $T_{2\omega}$ is the amplitude of temperature oscillation at frequency 2ω. Calibration experiments for the 3ω-wire method were performed for pure standard fluids, i.e., hydrocarbon (oil), fluorocarbon and water at ambient condition, and the system measurement uncertainty of k was $\pm$1.5%. It should be noted that the measurements of *p*H, viscosity, and thermal conductivity except the hydrodynamic size were made directly for the pristine colloid without any dilution.

III. RESULTS AND DISCUSSION

A. Kinetic control of silica colloid aggregation

As mentioned, when lowering the *p*H of the silica colloid from 10.1 up to the isoelectric point (*p*H$\approx$5.5), surface charge and repulsion potential are gradually reduced with respect to the invariant van der Waals attraction, which destabilizes the colloid. Near the IEP, strong interparticle attraction leads to aggregation resulting in ramified and self-similar fractal structures or even an entire percolating network.

The fractal nature of such aggregates is well characterized by a power law $M \propto R^{d_f}$, where M is mass of an aggregate, d_f is the fractal dimension, and R is the characteristic length of the aggregate [16–18]. Either radius of gyration R_g or hydrodynamic radius R_h can be used for the length R. Neglecting rotation of aggregates, R_h is defined as the size of an equivalent sphere that moves at the same velocity as the aggregate does and often is approximated by the size given from the DLS-measured translational diffusion coefficient through the Einstein-Stokes relation [19].

In terms of colloid aggregation kinetics, two limiting regimes are widely recognized: *fast* and *power-law-growth*
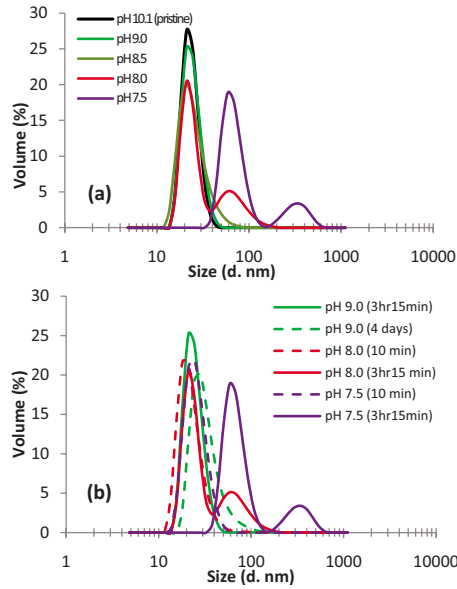
FIG. 1. (Color online) DLS size distributions for ST-40 silica colloids under controlled aggregation. (a) 3 h 15 min since initial pH adjustment except for the pristine case. The inset is viscosity evolution of the pH 8.0 and 7.5 samples. (b) Size evolution of silica clusters under controlled aggregation.

diffusion-limited colloid aggregation (DLCA) where the potential barrier is small relative to the thermal agitation $k_B T$, and *slow* and *exponential-growth* reaction-limited colloid aggregation (RLCA) where the energy barrier is comparable to or higher than $k_B T$.

Figure 1(a) shows the hydrodynamic size distributions of colloidal particles at different pHs. At $8.5 \leq p\text{H} \leq 10.1$, the size distribution profiles are nearly the same suggesting that colloidal spherical particles are well dispersed without any obvious aggregation over 3 h. At pH=8.0, an additional small peak appears at 72.6 nm while the first modal size is invariant, which implies that around 20%–30% of primary particles undergo a mild aggregation to form the second mode. At pH=7.5, however, the modal diameters greatly increase to around 67 and 336.5 nm with volume ratio of ca. 4 to 1. The inset figure of Fig. 1(a) shows the evolution of apparent viscosity of silica colloids at pHs of 8.0 and 7.5. The viscosity at pH=7.5 is rapidly increasing with time and always much higher than that at pH=8.0 representing that severe aggregation proceeds as compared to the case at pH=8.0. This is consistent with the size variations as shown in Fig. 1(a).

The pH effect on aggregation kinetics was further exploited by characterizing the size evolution with time as seen in Fig. 1(b). At pH=9.0, the colloid remains very stable as evidenced by the minimal change in size after four days. In contrast, at pH=8.0, as the additional peak in Fig. 1(a) did not appear at 10 min, the peak results from the aggregation process during the following 3 h, which might correspond to the relatively small increase in viscosity of the same sample in the inset of Fig. 1(a). At pH=7.5, aggregation was confirmed to be much more significant in 3 h, which is qualitatively consistent with the significant increase in the viscosity within 3 h. It should be noted that the size distributions at all
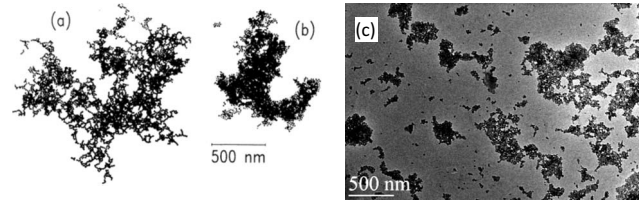

FIG. 2. TEM images of Au clusters aggregated through (a) DLCA, (b) RLCA [22], and aggregated ST-40 silica colloid at pH=7.5 after 3 h 15 min.

pH values are very similar at 10 min implying that the size measurement is reliable. Further observation until gelation shows that samples of pH 9, 8.5, 8.0, and 7.5 entirely gel to form a percolating structure after a course of ca. 360, 70, 14, and 4 h, respectively.

Returning to the aggregation regimes of RLCA and DLCA, extensive previous research [20–27] have reported two different typical values of fractal dimension, i.e., d_f = 1.86 ± 0.05 and 2.1 ± 0.05 for DLCA and RLCA, respectively. Also, different ratios of R_h/R_g of 0.765 and 1.0 for DLCA and RLCA have been reported, respectively, for silica, gold, and polystyrene latex colloidal systems [25,28,29]. It is well known that the RLCA process typically produces more compact aggregates with higher d_f than the DLCA, which is caused by the lower sticking probability. Numerical simulation indicates that more compact aggregates are often generated at high suspension concentration [26]. Regarding the present high volume loading, it is reasonable to assume that our aggregation process corresponds to the RLCA rather than the DLCA. Interestingly, Fig. 2 shows that the sample morphology at pH=7.5 [Fig. 2(c)] where the colloid was most unstable is very similar to that of gold clusters derived through RLCA in Fig. 2(b) rather than through DLCA in Fig. 2(a). Hence, the aggregation process might be close to the RLCA in the present condition, so that a d_f of 2.15 and R_h/R_g of 1.0 corresponding to RLCA are taken in this study and will be used in the modeling later.

B. General model for prediction of thermal conductivity

In this section, the Maxwell-Garnett effective medium theory is considered for spherical nonaggregated particles for $p\text{H} \geq 8.5$, and a fractal model considered for aggregates at pH=7.5 and 8.0. In general the M-G model is a combination of the H-C model and thermal boundary resistance, so that the effective thermal conductivity k of well dispersed spherical particles in a base fluid is expressed as [30]

$$\frac{k}{k_f} = \frac{1 + 2\beta\phi}{1 - \beta\phi}, \quad \beta = \frac{k_p(1-\alpha) - k_f}{k_p(1+2\alpha) + 2k_f}, \quad (1)$$

where ϕ is particle volume fraction and k_f, k_p, and k denote the thermal conductivity of the base fluid, particles, and the nanofluids, respectively. The solid-liquid interfacial thermal resistance or Kapitza resistance R_b is implicitly included in Eq. (1) through the nanoparticle Biot number α ($=2 R_b k_f / d_p$, where d_p denotes nanoparticle diameter). In the present

model calculation, we considered two values of R_b, i.e., 0 and 0.77×10^{-8} K m^2 W^{-1} as two limiting cases to evaluate the effect of R_b. The latter value has been indeed suggested as a good approximation for hydrophilic interface [31].

For aggregates, we adopted a model developed by Prasher *et al.* [4] to account for interfacial thermal resistance, Brownian motion-induced microconvection, and heat percolation due to nanoparticle clustering. The model combines both convective and conductive contributions and is given by

$$\frac{k}{k_f} = (1 + A \, \mathrm{Re}^\gamma \, \mathrm{Pr}^{0.333} \, \phi)\left(\frac{1 + 2\beta\phi}{1 - \beta\phi}\right). \qquad (2)$$

The first term in the right-hand side of Eq. (2) represents the convective contribution $(k/k_f)_{\mathrm{conv}}$ and the second term the conductive contribution $(k/k_f)_{\mathrm{cond}}$. Further, Re and Pr denote the Reynolds number for nanoparticles and the Prandtl number for fluid, respectively; $A = 4 \times 10^4$ is a fluid type-independent constant; γ is a system-specific exponent. A and γ should be unchanged for a particular fluid. The particle Reynolds number is expressed as

$$\mathrm{Re} = Vd/\nu = \frac{1}{\nu}\sqrt{\frac{18k_bT}{\pi\rho d}},$$

where ν is kinematic viscosity of base fluid, k_b is the Boltzmann constant, and ρ and d are density and diameter of particles, respectively. To apply Eq. (2) for fractal aggregates, the diameter d is substituted by a volume equivalent size d_{eq} of an aggregate that is defined by the diameter of a sphere that has the same volume of the aggregate as

$$d_{eq} = d_p\left(\frac{2R_g}{d_p}\right)^{d_f/3},$$

where R_g represents the average gyration radius of aggregates and d_p the diameter of primary (pristine spherical) particle. In addition, we have to modify the terms of β and ϕ in Eq. (2) for aggregate system. First we deal with an aggregate bounded by a spherical boundary as another equivalent sphere. The equivalent sphere then replaces the fractal aggregate. We have to know the thermal conductivity of such a sphere k_a and the volume fraction of solid phase in the sphere ϕ_{int}. According to fractal geometry, ϕ_{int} is expressed by

$$\phi_{\mathrm{int}} = \left(\frac{2R_g}{d_p}\right)^{d_f - 3}.$$

Then k_a is derived from the following relation based on the Bruggeman model as

$$(1 - \phi_{\mathrm{int}})(k_f - k_a)/(k_f + 2k_a) + \phi_{\mathrm{int}}(k_p - k_a)/(k_p + 2k_a) = 0.$$

Note that the total number of the artificial spheres is exactly the same as that of aggregates. Thus, the volume fraction of solid phase ϕ in Eq. (2) needs to be corrected with the volume fraction of the equivalent spheres ϕ_a in the whole fluid body as $\phi = \phi_{\mathrm{int}} \phi_a$. This will give rise to the increase in effective volume fraction from ϕ to ϕ_a in Eq. (2), decrease in thermal conductivity of the spheres k_a from k_p (i.e., $k_{\mathrm{SiO}_2} = 1.4$ W m^{-1} K^{-1}) to $k_{\mathrm{H}_2\mathrm{O}}$ (i.e., $k_{\mathrm{H}_2\mathrm{O}} < k_a < k_{\mathrm{SiO}_2}$), and de-
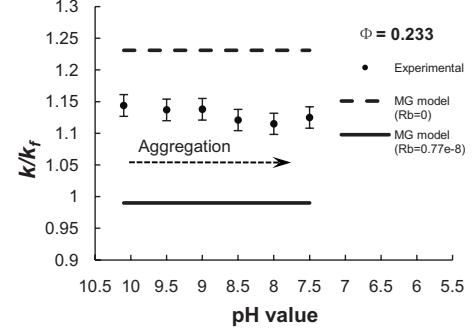

FIG. 3. Thermal conductivity of ST-40 silica colloids under controlled aggregation measured using 3ω-wire technique. Monodisperse pristine stock colloid (pH = 10.1, $\sim$15 nm) has a volume fraction of 0.233. Measurements were taken 3 h 15 min since initial pH adjustment except for the pristine case. Dashed and solid lines indicate results predicted by the M-G model. Typical measurement uncertainty of k is within $\pm 1.5\%$.

crease in Re by replacing d with d_{eq}. Finally, the conductive contribution $(k/k_f)_{\mathrm{cond}}$ and the convective contribution $(k/k_f)_{\mathrm{conv}}$ in an aggregated system can be determined by Eq. (2).

C. Effect of clustering on the effective thermal conductivity

Figure 3 shows the measured thermal conductivity of a series of destabilized ST-40 colloids whose size profiles are shown in Fig. 1(a). The experimental data are well bounded by the M-G model predictions with and without R_b. As the M-G model is valid for well dispersed spherical particle suspension, the measured thermal conductivity at pH = 10.1 (the pristine colloid) should be useful for evaluation of the model. The 15% increase in the effective thermal conductivity seems to be surmounted completely by the effect of the interfacial resistance (up to $\sim$23%). Also though pH decreases, there is no apparent effect of particle clustering, which is not in accord with the suggestion of Prasher *et al.* [32] and more recent work [33]. This surprising result might come from the low inherent thermal conductivity of silica material and/or because the minor benefit of clustering is completely compensated by the concomitant degradation of the convective contribution.

To clarify the conjectures, the fractal model in Eq. (2) was used. Table I lists the effective thermal conductivity predicted by the model along with various parameters for the pH 8.0 and 7.5 samples. The table shows that the increase in conductive contribution when decreasing pH from 8.0 to 7.5 is compensated by the decrease in the convective part due to the particle growth and the predicted k/k_f values are therefore quite close to experimental data for both samples, e.g., 1.1177 vs 1.115 for pH 8.0 and 1.1128 vs 1.125 for pH 7.5 sample. Note that the bimodal size profiles in Fig. 1 at such pHs were further simplified by assuming each system to consist of two monodisperse particle ensembles, the sizes of which are approximated by the weighted average sizes of the corresponding peak from each peak area in Fig. 1(a). It is also worth mentioning that rather than scattering intensity,

TABLE I. Modeled thermal conductivities of ST-40 silica colloids destabilized for 3 h 15 min since the initial pH adjustment. Values given in parentheses at the bottom are the corresponding experimental data. Data at the left and right columns for each pH correspond to the values for the first and second mode particles in Fig. 1(a), respectively.

	pH=8.0		pH=7.5	
	(RLCA, d_f=2.15)		(RLCA, d_f=2.15)	
$R_h \times 2$ (nm)	23.0	72.6	67.0	336.5
Vol. (%)	71.6	28.4	82.2	17.8
$R_g \times 2$ (nm)	23.0	72.6	67.0	336.5
d_{eq} (nm)	20.4	46.4	43.8	139.4
Re	0.0227	0.0150	0.0155	0.0087
Pr	6.990	6.990	6.990	6.990
α	0.402	0.127	0.138	0.027
Φ_{int}	0.695	0.262	0.280	0.071
Φ_a	0.291	0.115	0.787	0.170
k_a (W m^{-1} K^{-1})	1.112	0.764	0.777	0.641
β	0.020	0.031	0.032	0.012
$(k/k_f)_{cond}$	1.0179	1.0107	1.0771	1.0063
$(k/k_f)_{conv}$	1.0828	1.0033	1.0264	1.0002
k/k_f	1.1177 (vs 1.115)		1.1128 (vs 1.125)	

volumetric distribution of clusters has been obtained and used for the modeling purpose.

Based on the measured effective thermal conductivity (k/k_f=1.144) of the unaggregated pristine ST-40 sample (pH=10.1, 23.3 vol %, ~15 nm) and the incorporated conductive contribution $(k/k_f)_{cond}$ [calculated to be 0.99 using Eq. (1)], the system-specific constant (γ) in the convective part $(k/k_f)_{conv}$ of Eq. (2) was derived to be 3.205, which is not in the range of previously reported $2.5 \pm 15\%$ for CuO and Al$_2$O$_3$ nanofluids [34], but agrees very well with our fitted value (i.e., γ=3.267) based on another reported thermal conductivity data of Ludox silica colloid (~16.5 nm, 16 vol % and k/k_f=1.075) [35]. Thus, it would be very interesting to verify the behavior of the particle clustering effect when changing the thermal conductivity and microstructure of particles and is the focus of the remainder of the paper.

D. Tailoring thermal conductivity by changing thermal property and structure of particles

Figures 4(a) and 4(b) show that the particle clustering effect is indeed important when the particle material has a thermal conductivity higher than 10, and the effect is more pronounced when the factor of interfacial resistance is considered upon comparing Figs. 4(a) and 4(b). Note that the calculations are made under the assumption that all parameters are identical with the ST-40 with the only exception of the k_p. A possible explanation for the result might be that high-conducting materials with respect to silica are superior in gaining the conductive benefit while maintaining the convective contribution constant. This is better verified by sepa-
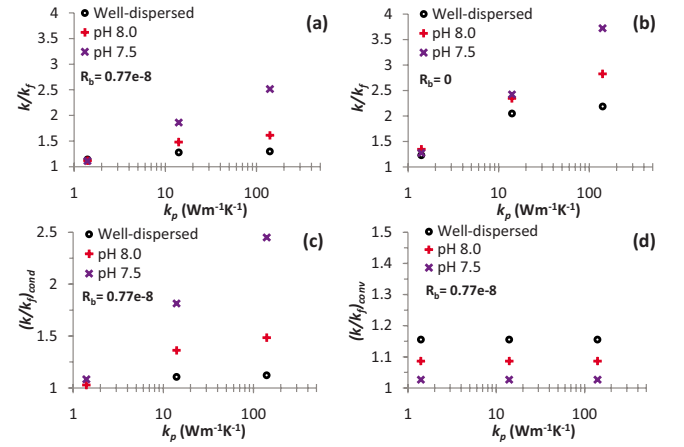

FIG. 4. (Color online) Influence of particle conductivity and interfacial thermal resistance R_b on the effective thermal conductivity of nanofluids in aggregated system. Set of k/k_f data corresponding to k_p=1.4, 14, and 140 W m^{-1} K^{-1} are model-predicted values at (a) R_b=0.77$\times$10^{-8} K m^2 W^{-1} and (b) R_b=0. The constituent conductive and convective parts of the total thermal conductivity for case (a) are shown in (c) and (d), respectively. Note that the cases with k_p=14 and 140 W m^{-1} K^{-1} are theoretical materials with all the same properties as ST-40 including aggregation kinetics and solid particle loading (ϕ=0.233), with the only exception of the inherent thermal conductivity of particle material.

rating the conductive and convective contributions to the effective thermal conductivity as shown in Figs. 4(c) and 4(d). Interestingly, the conductive contribution, or percolation effect, rapidly increases as the k_p begins to increase and then becomes gradually degraded with further increase in the k_p. Such a saturation seems to occur at relatively lower k_p for the less aggregated system (pH=8.0). Moreover, it is obvious that the conductive contribution dominates the thermal conductivity at $k_p \gtrsim 10$ suggesting that higher-conducting material is more desirable to shadow the interfacial resistance to obtain the clustering benefit.

Using the model, we have also studied the influence of fractal dimension d_f on the effective thermal conductivity for specific sizes of colloidal aggregates as shown in Fig. 5. Overall, the role of clustering is manifested to be positive. Figure 5(a), representing the silica colloid, shows that a higher d_f (denser structure) results in a slight increase in the
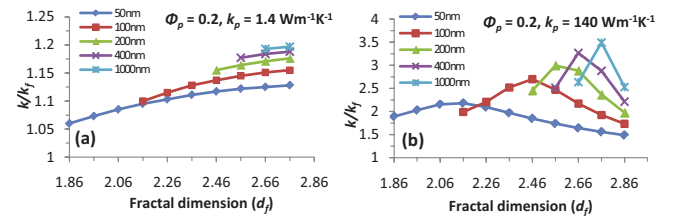

FIG. 5. (Color online) Effect of cluster fractal dimension d_f on the effective thermal conductivity of aggregated suspension (initiated from 15 nm monodisperse system) of silica (a) (k_p=1.4 W m^{-1} K^{-1}) and (b) theoretical material (k_p=140 W m^{-1} K^{-1}). Interfacial resistance R_b of 0.77e-8 K m^2 W^{-1} was used and the numbers in the legends stand for diameters of gyration ($2R_g$) of fractals.

k at the constant aggregate size. Note that only a higher d_f part was displayed for larger aggregates; for example, for 1000 nm aggregates, if d_f decreases over 2.6 (toward a more open structure) while keeping the number and size of aggregates constant, the volume fraction of aggregates (ϕ_a) can increase over 1.0, which is unpractical and thus not displayed. Figure 5(b) shows that in a theoretical high-conducting material system, there exists an optimum d_f value for maximum enhancement. Given the fixed aggregate size, although the k_a (the thermal conductivity of an aggregate) and the ϕ_{int} (volume fraction of solid fraction inside the equivalent sphere bounding the aggregate) increase in more compact aggregate, the ϕ_a (the effective volume fraction of aggregates) should decrease to maintaining the ϕ constant (=0.2). For example, in a 200 nm aggregate system, when d_f increases from 2.56 to 2.66, the convective contribution slightly decreases due to a little increase in mass of aggregate; whereas, the conductive part is obviously degraded mainly by a decrease in ϕ_a from 0.63 to 0.48, rather than by the increase in either k_a (from 5.35 to 19.43) or ϕ_{int} (from 0.32 to 0.41). Figure 5(b) also shows that for the constant d_f, larger aggregate does not always give higher thermal conductivity as described above. This is why the optimal control of aggregation is crucial to maximize the benefit of particle clustering.

IV. CONCLUSIONS

Starting with a well-defined system followed by accurate control of aggregation state, we have explored both theoretically and experimentally nanoparticle clustering effects on the effective thermal conductivity in nanofluids. Contrary to the previous model prediction, i.e., the twofold increase in the effective thermal conductivity of best-clustered Al_2O_3 nanofluid with respect to the well-suspended system, the present experiment showed that the clustering did not give rise to any distinct difference in the k for less-conducting SiO_2 nanofluid even at unusually high volume loading of ~23%. A generalized fractal model suggested that the conductive benefit due to clustering might be completely compensated by the reduced convective contribution due to particle growth. A series of parametric model predictions revealed that higher thermal conductivity and optimized fractal dimension of particles were required for maximizing the clustering effect.

[1] J. C. Maxwell Garnett, Philos. Trans. R. Soc. London, Ser. A **203**, 385 (1904).

[2] D. A. G. Bruggeman, Ann. Phys. **416**, 636 (1935).

[3] R. L. Hamilton and O. K. Crosser, Ind. Eng. Chem. Fundam. **1**, 187 (1962).

[4] R. Prasher, P. E. Phelan, and P. Bhattacharya, Nano Lett. **6**, 1529 (2006).

[5] B. Wang, L. Zhou, and X. Peng, Int. J. Heat Mass Transfer **46**, 2665 (2003).

[6] P. Keblinski, S. R. Phillpot, S. U. S. Choi, and J. A. Eastman, Int. J. Heat Mass Transfer **45**, 855 (2002).

[7] S. P. Jang and S. U. S. Choi, Appl. Phys. Lett. **84**, 4316 (2004).

[8] S. Krishnamurthy, P. Bhattacharya, P. E. Phelan, and R. S. Prasher, Nano Lett. **6**, 419 (2006).

[9] R. Prasher, P. Bhattacharya, and P. E. Phelan, Phys. Rev. Lett. **94**, 025901 (2005).

[10] T.-H. Tsai, L.-S. Kuo, P.-H. Chen, and C.-T. Yang, Appl. Phys. Lett. **93**, 233121 (2008).

[11] D. Lee, Langmuir **23**, 6011 (2007).

[12] D. S. McLachlan, M. Blaszkiewicz, and R. E. Newnham, J. Am. Ceram. Soc. **73**, 2187 (1990).

[13] D. S. McLachlan, J. Phys. C **20**, 865 (1987).

[14] E. V. Timofeeva, A. N. Gavrilov, J. M. McCloskey, Y. V. Tolmachev, S. Sprunt, L. M. Lopatina, and J. V. Selinger, Phys. Rev. E **76**, 061203 (2007).

[15] Z. H. Han, B. Yang, S. H. Kim, and M. R. Zachariah, Nanotechnology **18**, 105701 (2007); I. E. Yusibani, P. L. Woodfield, M. Fujii, K. Shinzato, X. Zhang, and Y. Takat, Int. J. Thermophys. **30**, 397 (2009).

[16] S. R. Forrest and T. A. Witten, J. Phys. A **12**, L109 (1979).

[17] T. A. Witten and L. M. Sander, Phys. Rev. Lett. **47**, 1400 (1981).

[18] C. M. Sorensen, Aerosol Sci. Technol. **35**, 648 (2001).

[19] H. M. Lindsay, M. Y. Lin, D. A. Weitz, R. C. Ball, R. Klein, and P. Meakin, Proceedings of the Photon Correlation Techniques and Applications, edited by J. B. Abbiss and A. E. Smart (Optical Society of America, Washington, DC, 1988), Vol. 1, p. 122.

[20] D. W. Schaefer, J. E. Martin, P. Wiltzius, and D. S. Cannell, Phys. Rev. Lett. **52**, 2371 (1984).

[21] C. Aubert and D. S. Cannell, Phys. Rev. Lett. **56**, 738 (1986).

[22] D. A. Weitz, J. S. Huang, M. Y. Lin, and J. Sung, Phys. Rev. Lett. **54**, 1416 (1985).

[23] P. Meakin, Phys. Rev. Lett. **51**, 1119 (1983).

[24] M. Kolb, R. Botet, and J. Jullien, Phys. Rev. Lett. **51**, 1123 (1983).

[25] P. Wiltzius, Phys. Rev. Lett. **58**, 710 (1987).

[26] T. P. M. Beelen, W. H. Dokter, H. F. Van Garderen, and R. A. Van Santen, Adv. Colloid Interface Sci. **50**, 23 (1994).

[27] M. Y. Lin, H. M. Lindsay, D. A. Weitz, R. C. Ball, R. Klein, and P. Meakin, Phys. Rev. A **41**, 2005 (1990).

[28] P. N. Pusey, J. G. Rarity, R. Klein, and D. A. Weitz, Phys. Rev. Lett. **59**, 2122 (1987).

[29] M. Lattuada, H. Wu, and M. Morbidelli, J. Colloid Interface Sci. **268**, 96 (2003).

[30] J. Eapen, W. C. Williams, J. Buongiorno, L. Hu, and S. Yip, Phys. Rev. Lett. **99**, 095901 (2007).

[31] O. M. Wilson, X. Hu, D. G. Cahill, and P. V. Braun, Phys. Rev. B **66**, 224301 (2002).

[32] W. Evans, R. Prasher, J. Fish, P. Meakin, P. Phelan, and P. Keblinski, Int. J. Heat Mass Transfer **51**, 1431 (2008).

[33] P. Keblinski, R. Prasher, and J. Eapen, J. Nanopart. Res. **10**, 1089 (2008).

[34] R. Prasher, P. Bhattacharya, and P. E. Phelan, ASME J. Heat Transfer **128**, 588 (2006).

[35] G. Chen, W. Yu, D. Singh, D. Cookson, and J. Routbort, J. Nanopart. Res. **10**, 1109 (2008).